

the atmosphere (31, 32). The style of activity imaged requires that the observed slipfaces are not strongly ice-cemented within the erosion depths. Some of the new grainflow alcoves have widths of tens of meters and have recessed in excess of 10 m into the brink. This implies transport of hundreds of cubic meters of sand (fig. S1). Even intermediate-sized gullies such as that in Fig. 5 require movement of tens of cubic meters of sediment.

The reworking of older gully alcoves by aeolian ripples is shown in Fig. 5. The recovery rate of the slipface and the existence of smooth slopes (no grainflows) suggests that grainflow formation and remobilization of sediment by wind may be approximately in equilibrium on a multiyear time scale, although relative rates could vary annually. The seasonal-scale frequency of these two processes demonstrates active sediment transport on polar dunes in the current martian climate. Whether they indicate migration of martian dune forms or simply represent the crestline maintenance of nonmobile dunes can only be determined with future multiyear observations.

In locations where wind energy is insufficient to reconstitute grainflow scars, modification of dune form should ensue. With an estimated sediment transport that delivers tens to hundreds of cubic meters of sand in one Mars year to the dune foot slopes, the initial modification of dune form would be rapid. Resulting dune morphologies would have rounded crests, no brinks, and long, low-angle footslopes. This mechanism may explain some of the unusual dune forms reported on Mars (33). However, because the majority of Mars' north polar dunes do not assume this morphology, we suggest that maintenance of the

dune form is an active process under the current martian climate.

References and Notes

- M. R. Balme, D. Berman, M. Bourke, J. Zimbelman, *Geomorphology* **101**, 703 (2008).
- J. F. McCauley *et al.*, *Icarus* **17**, 289 (1972).
- J. A. Cutts, R. S. U. Smith, *J. Geophys. Res.* **78**, 4139 (1973).
- H. Tsoar, R. Greeley, A. R. Peterfreund, *J. Geophys. Res.* **84** (B14), 8167 (1979).
- A. W. Ward, K. B. Doyle, *Icarus* **55**, 420 (1983).
- M. C. Bourke, K. Edgett, B. Cantor, *Geomorphology* **94**, 247 (2008).
- M. C. Bourke *et al.*, *Proc. Lunar Planet. Sci. Conf.* **40**, 1748 (2009).
- V. Schatz, H. Tsoar, K. S. Edgett, E. J. R. Parteli, H. J. Herrmann, *J. Geophys. Res.* **111** (E4), E002514 (2006).
- In this paper, we use "frost" and "ice" somewhat interchangeably. Martian snow has been shown to increase in density as the winter season progresses (34), so usage of this terminology transitions from one to the other. Readers are encouraged to understand the use of either term to be synonymous with "seasonally condensed volatile."
- M. Malin, K. Edgett, *J. Geophys. Res.* **106** (E10), 23429 (2001).
- C. J. Hansen *et al.*, *Bull. Am. Astron. Soc.* **40**, 409 (2008).
- The numbering of Mars years was defined to facilitate comparison of data sets across decades and multiple Mars missions. Year 1 started 11 April 1955.
- A. McEwen *et al.*, *J. Geophys. Res.* **112** (E5), E002605 (2007).
- A. Kereszturi *et al.*, *Icarus* **201**, 492 (2009).
- A. Kereszturi *et al.*, *Icarus* **207**, 149 (2010).
- D. Möhlmann, A. Kereszturi, *Icarus* **207**, 654 (2010).
- C. Hansen *et al.*, *Proc. Lunar Planet. Sci. Conf.* **41**, 1533 (2010).
- M. C. Malin, K. Edgett, NASA/JPL Planetary Photojournal, <http://photojournal.jpl.nasa.gov/>, catalog no. PIA04290 (2005).
- S. Diniega, S. Byrne, N. T. Bridges, C. M. Dundas, A. S. McEwen, *Geology* **38**, 1047 (2010).

- E. Gardin, P. Allemand, C. Quantin, P. Thollot, *J. Geophys. Res.* **115** (E6), E06016 (2010).
- C. M. Dundas, A. S. McEwen, S. Diniega, S. Byrne, S. Martinez-Alonso, *Geophys. Res. Lett.* **37**, L07202 (2009).
- H. H. Kieffer, Lunar and Planetary Institute contribution 1057 (2000).
- S. Piqueux, P. R. Christensen, *J. Geophys. Res.* **113** (E6), E06005 (2003).
- O. Aharonson, 35th Lunar and Planetary Science Conference, 15 to 19 March 2004, League City, TX, abstr. 1918 (2004).
- H. Kieffer, *J. Geophys. Res.* **112** (E8), E08005 (2007).
- S. Piqueux, P. R. Christensen, *J. Geophys. Res.* **113** (E6), E06005 (2008).
- C. J. Hansen *et al.*, *Icarus* **205**, 283 (2010).
- N. Thomas, C. J. Hansen, G. Portyankina, P. S. Russell, *Icarus* **205**, 296 (2010).
- G. Portyankina, W. J. Markiewicz, N. Thomas, C. J. Hansen, M. Milazzo, *Icarus* **205**, 311 (2010).
- S. Silvestro *et al.*, *Second International Dunes Conference, LPI Contributions*, **1552**, 65 (2010).
- M. Mellon *et al.*, *J. Geophys. Res.* **114**, E00E07 (2009).
- N. Putzig *et al.*, *Proc. Lunar Planet. Sci. Conf.* **41**, 1533 (2010).
- R. Hayward *et al.*, *J. Geophys. Res.* **112** (E11), E11007 (2007).
- K. Matsuo, K. Heki, *Icarus* **202**, 90 (2009).
- L_s is the true anomaly of Mars in its orbit around the sun, measured from the martian vernal equinox, used as a measure of the season on Mars. $L_s = 0$ corresponds to the beginning of northern spring; $L_s = 180$ is the beginning of southern spring.
- This work was partially supported by the Jet Propulsion Laboratory, California Institute of Technology, under a contract with NASA.

Supporting Online Material

www.sciencemag.org/cgi/content/full/331/6017/575/DC1
SOM Text
Fig. S1
References

10 September 2010; accepted 10 January 2011
10.1126/science.1197636

2500 Years of European Climate Variability and Human Susceptibility

Ulf Büntgen,^{1,2*} Willy Tegel,³ Kurt Nicolussi,⁴ Michael McCormick,⁵ David Frank,^{1,2} Valerie Trouet,^{1,6} Jed O. Kaplan,⁷ Franz Herzig,⁸ Karl-Uwe Heussner,⁹ Heinz Wanner,² Jürg Luterbacher,¹⁰ Jan Esper¹¹

Climate variations influenced the agricultural productivity, health risk, and conflict level of preindustrial societies. Discrimination between environmental and anthropogenic impacts on past civilizations, however, remains difficult because of the paucity of high-resolution paleoclimatic evidence. We present tree ring–based reconstructions of central European summer precipitation and temperature variability over the past 2500 years. Recent warming is unprecedented, but modern hydroclimatic variations may have at times been exceeded in magnitude and duration. Wet and warm summers occurred during periods of Roman and medieval prosperity. Increased climate variability from ~250 to 600 C.E. coincided with the demise of the western Roman Empire and the turmoil of the Migration Period. Such historical data may provide a basis for counteracting the recent political and fiscal reluctance to mitigate projected climate change.

Continuing global warming and its potential associated threats to ecosystems and human health present a substantial challenge to modern civilizations that already experience many direct and indirect impacts of anthropogenic climate change (1–4). The rise and fall of

past civilizations have been associated with environmental change, mainly due to effects on water supply and agricultural productivity (5–9), human health (10), and civil conflict (11). Although many lines of evidence now point to climate forcing as one agent of distinct episodes of societal

crisis, linking environmental variability to human history is still limited by the dearth of high-resolution paleoclimatic data for periods earlier than 1000 years ago (12).

Archaeologists have developed oak (*Quercus* spp.) ring width chronologies from central Europe that cover nearly the entire Holocene and have used them for the purpose of dating archaeological artifacts, historical buildings, antique artwork, and furniture (13). The number of samples contributing to these records fluctuates between hundreds

¹Swiss Federal Research Institute for Forest, Snow and Landscape Research (WSL), 8903 Birmensdorf, Switzerland. ²Oeschger Centre for Climate Change Research, University of Bern, 3012 Bern, Switzerland. ³Institute for Forest Growth, University of Freiburg, 79085 Freiburg, Germany. ⁴Institute of Geography, University of Innsbruck, 6020 Innsbruck, Austria. ⁵Department of History, Harvard University, Cambridge, MA 02138, USA. ⁶Laboratory of Tree-Ring Research, University of Arizona, Tucson, AZ 85721, USA. ⁷Environmental Engineering Institute, École Polytechnique Fédérale de Lausanne, 1015 Lausanne, Switzerland. ⁸Bavarian State Department for Cultural Heritage, 86672 Thierhaupten, Germany. ⁹German Archaeological Institute, 14195 Berlin, Germany. ¹⁰Department of Geography, Justus Liebig University, 35390 Giessen, Germany. ¹¹Department of Geography, Johannes Gutenberg University, 55128 Mainz, Germany.

*To whom correspondence should be addressed. E-mail: buentgen@wsl.ch

and thousands in periods of societal prosperity, whereas fewer samples from periods of socioeconomic instability are available (14). Chronologies of living (15) and relict oaks (16, 17) may reflect distinct patterns of summer precipitation and drought if site ecology and local climatology imply moisture deficits during the vegetation period. Annually resolved climate reconstructions that contain long-term trends and extend prior to medieval times, however, depend not only on the inclusion of numerous ancient tree-ring samples of sufficient climate sensitivity, but also on frequency preservation, proxy calibration, and uncertainty estimation (18–20).

To better understand interannual to multicentennial changes in central European April-to-June (AMJ) precipitation over the late Holocene, we used 7284 precipitation-sensitive oak ring width series from subfossil, archaeological, historical, and recent material representing temperate forests in northeastern France (NEF), northeastern Germany (NEG), and southeastern Germany (SEG) (Fig. 1). We found that the mean annual replication was 286 series, with a maximum of 550 series during Roman times and the smallest sample size of 44 series at ~400 C.E. Growth variations among the three regions were significantly ($P < 0.001$) correlated over the past two millennia: NEF/SEG at 0.53, SEG/NEG at 0.47, and NEF/NEG at 0.37 (21). Correlation coefficients among AMJ precipitation readings from three stations in NEF, NEG, and SEG averaged 0.31 over the common instrumental

period (1921 to 1988), whereas the three regional oak chronologies correlated at 0.37 over the same interval (21).

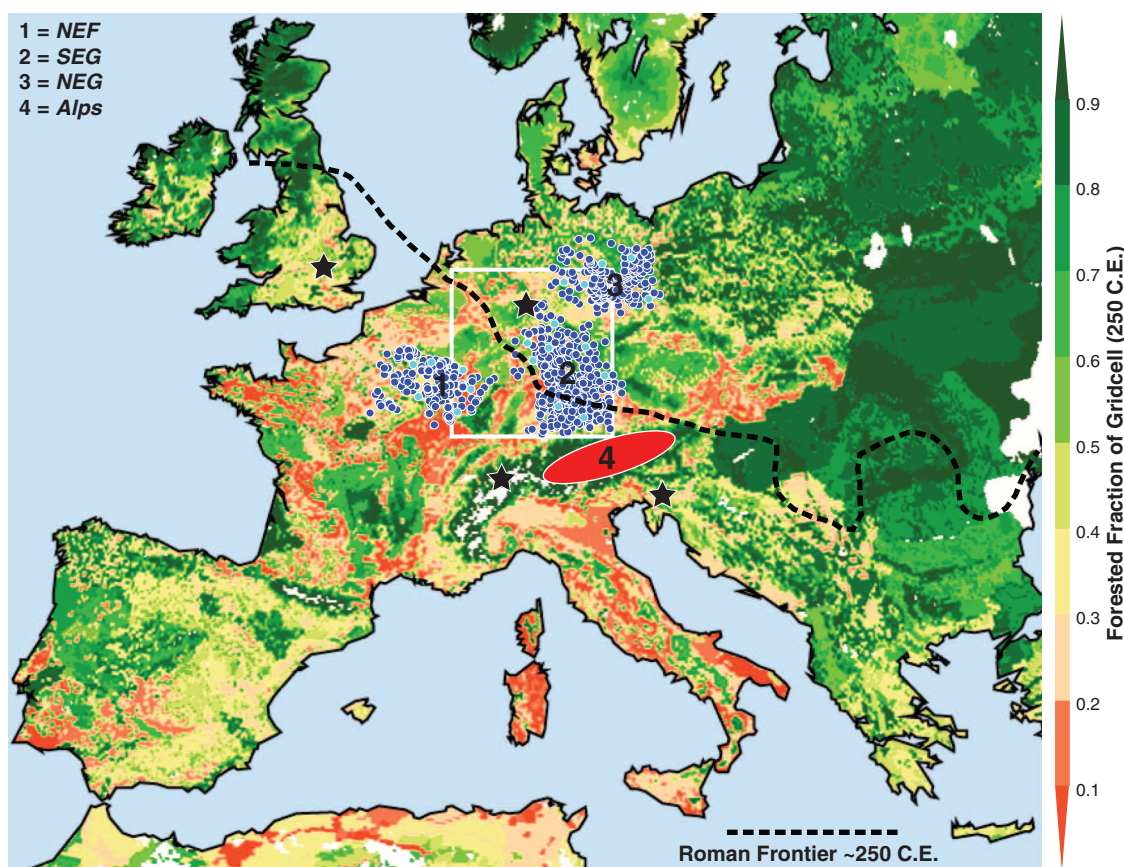
The temporal distribution of historical tree harvest (i.e., felling dates) mimics preindustrial deforestation and population trends (Fig. 2), implying substantial anthropogenic landscape perturbation over the last 2500 years (22). Increased felling dates reflect construction activity during the late Iron Age and Roman Empire (~300 B.C.E. to 200 C.E.) and indicate that the maximum expansion and deforestation of the Western Roman Empire (WRE) occurred around 250 C.E. Reduced tree harvesting at ~250 to 400 C.E. coincides with the biggest central European historical crisis, the Migration Period, a time marked by lasting political turmoil, cultural change, and socioeconomic instability (23, 24). Increasing timber harvest for construction is represented by abundant felling parallel to socioeconomic consolidation from the 6th to the 9th centuries C.E. Many earlier structures were replaced during a settlement boom in the 13th century (23, 24), eliminating much construction evidence from the central medieval period (900 to 1100 C.E.). Construction activity during the last millennium was disrupted by the Great Famine and Black Death (19) as well as by the Thirty Years' War.

To assess climatic drivers of oak growth during industrial and preindustrial times, we compared chronologies of high-frequency variability

with instrumental records, independent climate reconstructions, and historical archives (21). A total of 87 different medieval written sources comprise 88 eyewitness accounts of regional hydroclimatic conditions (with as many as seven reports per year) resolved to the year or better, which corroborate 30 out of 32 of the extremes preserved in our oak record between 1013 and 1504 C.E., whereas 16 reports were found to be contradictory (Fig. 3A). These observations further confirm the spatial signature of the climatic signal reflected by the oak network. Scaled precipitation anomaly composites calculated for the 12 most positive and the 16 most negative oak extremes back to 1500 C.E. revealed significantly wet and dry central European summers, respectively (Fig. 3B) (21). Independently derived extremes in pan-European oak growth over the last millennium match 5 of 11 extremes at the central European network level, and 21 of 53 at the regional scale (fig. S6).

The regional oak chronologies correlate on average at 0.39 with AMJ precipitation variability (1901–1980) averaged over 45° to 50°N and 8° to 10°E. Increased agreement between the tree-ring proxy and instrumental target records is obtained from the combined central European oak record, which correlates at 0.50 to 0.59 with interannual to multidecadal variations in AMJ precipitation (fig. S9). Correlation between this study and an independent summer drought reconstruction from central Germany (19) is 0.56

Fig. 1. Location of the 7284 central European oak samples (blue) and the network of 1546 Alpine conifers (red), superimposed on a deforestation model of Roman land use and land cover around 250 C.E. (22). Black stars indicate the location of the independent tree-ring chronologies used for comparison (16–19); the white box denotes the area over which gridded precipitation totals were averaged and used for proxy calibration.



over the common 996 to 2005 C.E. period (Fig. 4). To complement our hydroclimatic reconstruction, we also developed a central European summer temperature proxy based on 1089 stone pine (*Pinus cembra*) and 457 European larch (*Larix decidua*) ring width series from high-elevation sites in the Austrian Alps and adjacent areas (21). This composite record includes living trees, historical timber, and subfossil wood, and correlates at 0.72 to 0.92 with interannual to multidecadal variations in instrumental June-to-August (JJA) temperature (1864–2003). The new proxy is significantly positive correlated with 20th century JJA temperatures of central Europe and the Mediterranean region (21), and possesses high- to low-frequency agreement with an independent maximum latewood density-based temperature surrogate from the Swiss Alps (18) ($r = 0.35$ to 0.44; 755 to 2003 C.E.) (Fig. 4).

AMJ precipitation was generally above average and fluctuated within fairly narrow margins from the Late Iron Age through most of the Roman Period until ~250 C.E., whereas two depressions in JJA temperature coincided with the Celtic Expansion (~350 B.C.E.) and the Roman Conquest (~50 B.C.E.). Exceptional climate variability is reconstructed for ~250 to 550 C.E. and coincides with some of the most severe chal-

lenges in Europe's political, social, and economic history, during the Migration Period. Distinct drying in the 3rd century paralleled a period of serious crisis in the WRE marked by barbarian invasion, political turmoil, and economic dislocation in several provinces of Gaul, including Belgica, Germania superior, and Rhaetia (24, 25). Precipitation increased during the recovery of the WRE in the 300s under the dynasties of Constantine and Valentinian, while temperatures were below average. Precipitation surpassed early imperial levels during the demise of the WRE in the 5th century before dropping sharply in the first half of the 6th century. At the same time, falling lake levels in Europe and Africa (1, 26) accompanied hemispheric-scale cooling that has been linked with an explosive near-equatorial volcanic eruption in 536 C.E. (27), followed by the first pandemic of Justinian plague that spread from the eastern Mediterranean in 542–543 C.E. (28). Rapid climate changes together with frequent epidemics had the overall capacity to disrupt the food production of agrarian societies (5–8). Most of the oak samples from this period originate from archaeological excavations of water wells and subfossil remains currently located in floodplains and wetlands (Fig. 2D), possibly attesting to drier conditions during their colonization.

AMJ precipitation and JJA temperature began to increase from the end of the 6th century C.E. and reached climate conditions comparable to those of the Roman period in the early 800s. The onset of wetter and warmer summers is contemporaneous with the societal consolidation of new kingdoms that developed in the former WRE (23). Reduced climate variability from ~700 to 1000 C.E., relative to its surroundings, matches the new and sustained demographic growth in the northwest European countryside, and even the establishment of Norse colonies in the cold environments of Iceland and Greenland (9). Humid and mild summers paralleled the rapid cultural and political growth of medieval Europe under the Merovingian and Carolingian dynasties and their successors (23). Average precipitation and temperature showed fewer fluctuations during the period of peak medieval demographic and economic growth, ~1000 to 1200 C.E. (22, 23). Wetter summers during the 13th and 14th centuries and a first cold spell at ~1300 C.E. agree with the globally observed onset of the Little Ice Age (20, 29), likely contributing to widespread famine across central Europe. Unfavorable climate may have even played a role in debilitating the underlying health conditions that contributed to the

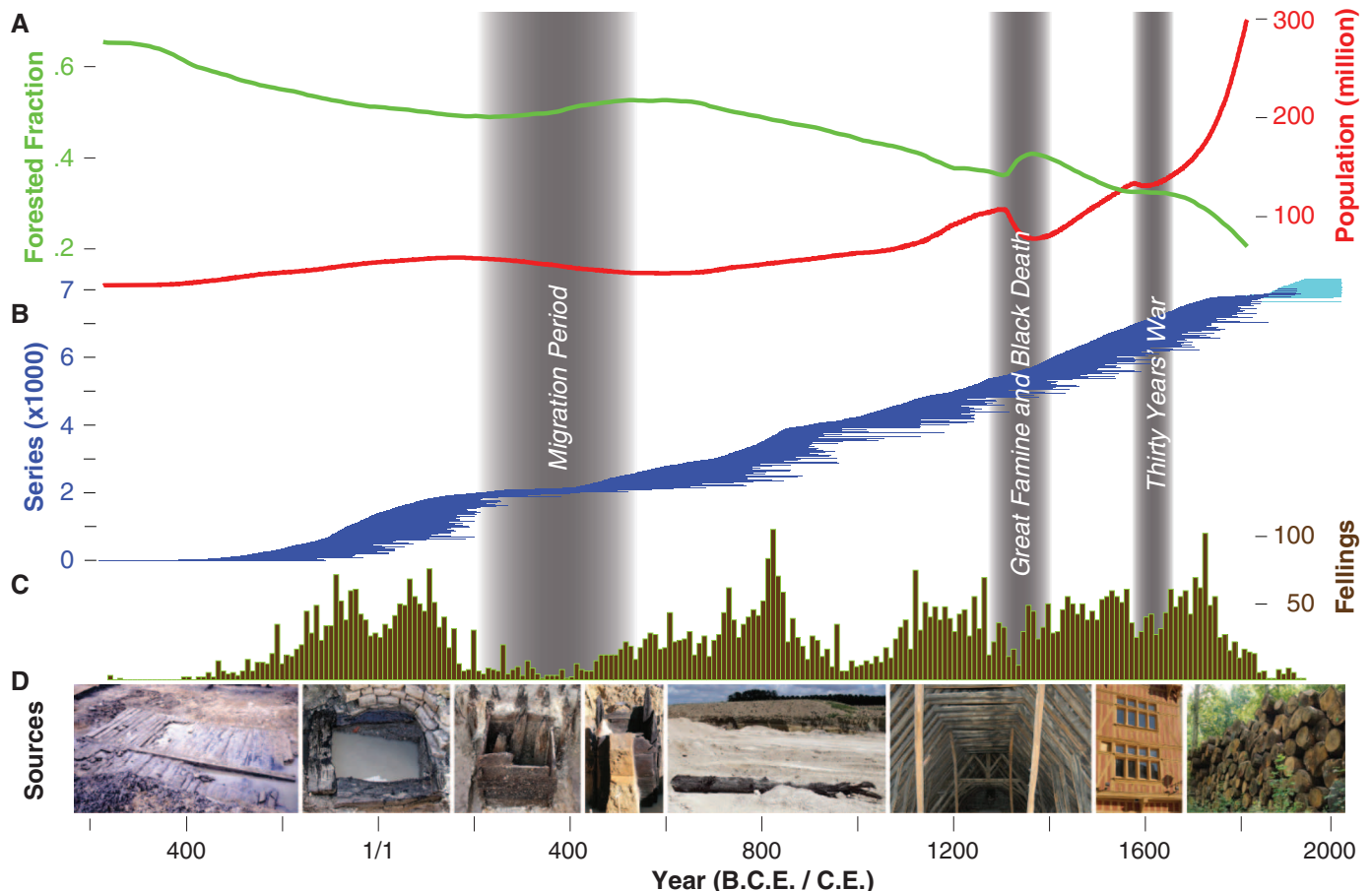


Fig. 2. (A to D) Evolution of central European forest cover and population from (22) (A), together with oak sample replication (B), their historical end dates at decadal resolution (C), and examples of archaeological (left), subfossil, historical, and recent (right) sample sources (D).

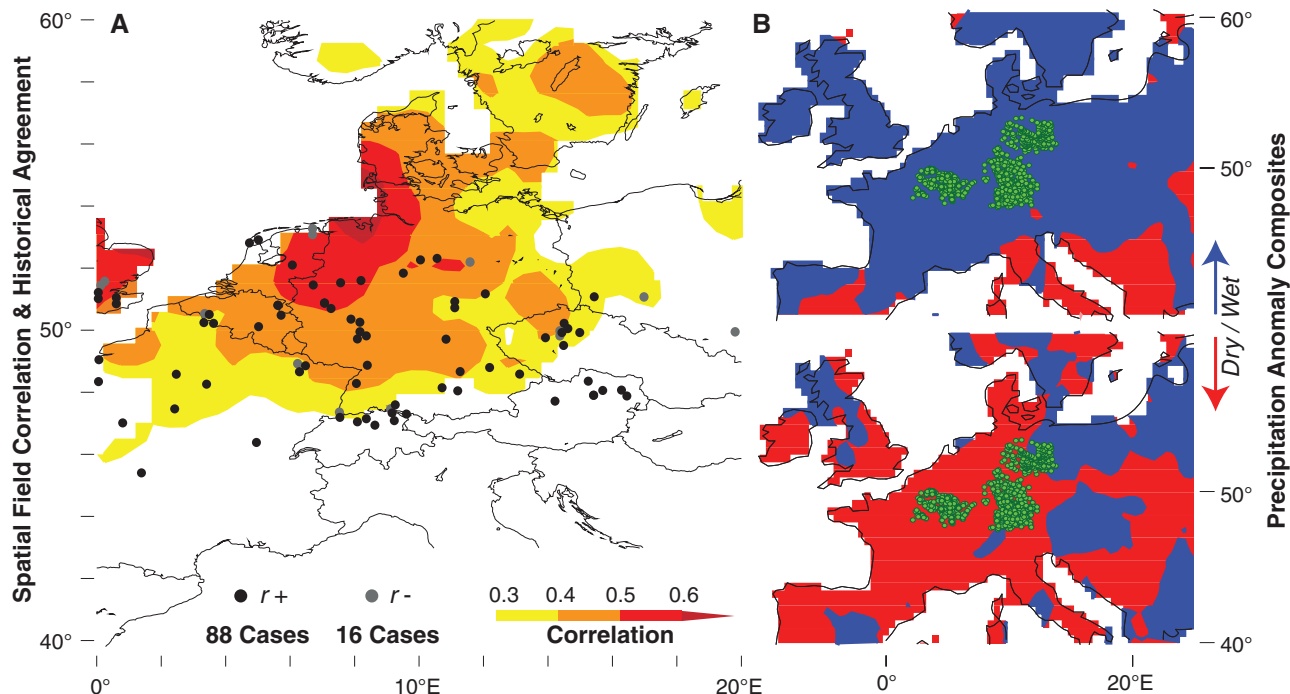


Fig. 3. (A) Correlation map of the mean oak chronology against gridded central European AMJ precipitation data (1901–1980) together with the location of 104 historical reports, of which 88 witnesses corroborate 30 of 32 climatic extremes that were reconstructed from the oak data between 1013 and 1504, whereas 16 witnesses offer contradictory reports. Note that different reports may originate from the same location. (B) Composite anomaly fields (scaled means, modified

t values) of summer (JJA) precipitation computed for 12 positive (top) and 16 negative (bottom) oak extremes between 1500 and 2000 (21). Significance of the composite anomalies, relative to the 1901–2000 climatology, was computed using 95% confidence thresholds of the modified two-sided t test (21). Blue and red colors refer to significantly wet and dry conditions, respectively. Green dots refer to the location of 7284 central European oak samples.

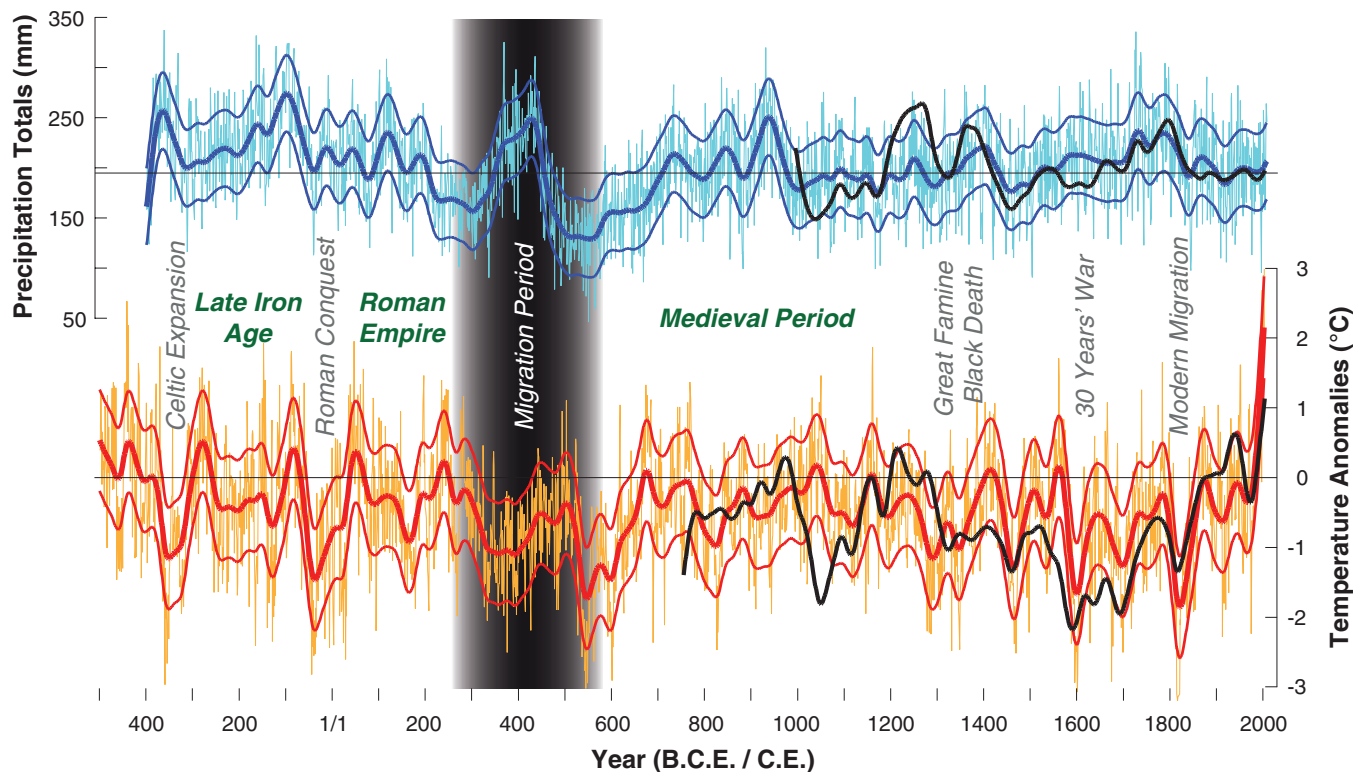


Fig. 4. Reconstructed AMJ precipitation totals (top) and JJA temperature anomalies (bottom) with respect to the 1901–2000 period. Error bars are ± 1 RMSE of the calibration periods. Black lines show independent precipitation and temperature reconstructions from Germany (19) and

Switzerland (18). Bold lines are 60-year low-pass filters. Periods of demographic expansion, economic prosperity, and societal stability are noted, as are periods of political turmoil, cultural change, and population instability.

Downloaded from www.sciencemag.org on February 3, 2011

devastating economic crisis that arose from the second plague pandemic, the Black Death, which reduced the central European population after 1347 C.E. by 40 to 60% (19, 22, 28). The period is also associated with a temperature decline in the North Atlantic and the abrupt desertion of former Greenland settlements (9). Temperature minima in the early 17th and 19th centuries accompanied sustained settlement abandonment during the Thirty Years' War and the modern migrations from Europe to America.

The rate of natural precipitation and temperature change during the Migration Period may represent a natural analog to rates of projected anthropogenic climate change. Although modern populations are potentially less vulnerable to climatic fluctuations than past societies have been, they also are certainly not immune to the predicted temperature and precipitation changes, especially considering that migration to more favorable habitats (22) as an adaptive response will not be an option in an increasingly crowded world (6). Comparison of climate variability and human history, however, prohibits any simple causal determination; other contributing factors such as sociocultural stressors must be considered in this complex interplay (7, 30). Nonetheless, the new climate evidence sets a paleoclimatic benchmark in terms of temporal resolution, sample replication, and record length.

Our data provide independent evidence that agrarian wealth and overall economic growth might be related to climate change on high- to mid-frequency (interannual to decadal) time scales. Preindustrial societies were sensitive to famine, disease, and war, which were often driven by drought, flood, frost or fire events, as independently described by documentary archives (30).

It also appears to be likely that societies can better compensate for abrupt (annual) climatic extremes and have the capacity to adapt to slower (multidecadal to centennial) environmental changes (6, 7).

The historical association of precipitation and temperature variation with population migration and settlement desertion in Europe may provide a basis for questioning the recent political and fiscal reluctance to mitigate projected global climate change (31), which reflects the common societal belief that civilizations are insulated from variations in the natural environment.

References and Notes

1. T. M. Shanahan *et al.*, *Science* **324**, 377 (2009).
2. E. R. Cook, R. Seager, M. A. Cane, D. W. Stahle, *Earth Sci. Rev.* **81**, 93 (2007).
3. M. E. Mann, J. D. Woodruff, J. P. Donnelly, Z. Zhang, *Nature* **460**, 880 (2009).
4. E. R. Cook *et al.*, *Science* **328**, 486 (2010).
5. B. M. Buckley *et al.*, *Proc. Natl. Acad. Sci. U.S.A.* **107**, 6748 (2010).
6. H. Weiss, R. S. Bradley, *Science* **291**, 609 (2001).
7. P. B. deMenocal, *Science* **292**, 667 (2001).
8. G. H. Haug *et al.*, *Science* **299**, 1731 (2003).
9. W. P. Patterson, K. A. Dietrich, C. Holmden, J. T. Andrews, *Proc. Natl. Acad. Sci. U.S.A.* **107**, 5306 (2010).
10. A. J. McMichael, R. E. Woodruff, S. Hales, *Lancet* **367**, 859 (2006).
11. M. B. Burke, E. Miguel, S. Satyanath, J. A. Dykema, D. B. Lobell, *Proc. Natl. Acad. Sci. U.S.A.* **106**, 20670 (2009).
12. P. D. Jones *et al.*, *Holocene* **19**, 3 (2009).
13. K. Haneca, K. Ćufar, H. Beekman, *J. Archaeol. Sci.* **36**, 1 (2009).
14. W. Tegel, J. Vanmoerkerke, U. Büntgen, *Quat. Sci. Rev.* **29**, 1957 (2010).
15. D. A. Friedrichs *et al.*, *Tree Physiol.* **29**, 39 (2009).
16. P. M. Kelly, H. H. Leuschner, K. R. Briffa, I. C. Harris, *Holocene* **12**, 689 (2002).
17. K. Ćufar, M. De Luis, D. Eckstein, L. Kajfez-Bogataj, *Int. J. Biometeorol.* **52**, 607 (2008).

18. U. Büntgen, D. C. Frank, D. Nievergelt, J. Esper, *J. Clim.* **19**, 5606 (2006).
19. U. Büntgen *et al.*, *Quat. Sci. Rev.* **29**, 1005 (2010).
20. D. C. Frank *et al.*, *Nature* **463**, 527 (2010).
21. See supporting material on Science Online.
22. J. O. Kaplan, K. M. Krumhardt, N. Zimmermann, *Quat. Sci. Rev.* **28**, 3016 (2009).
23. M. McCormick, *Origins of the European Economy: Communications and Commerce, A.D. 300–900* (Cambridge Univ. Press, Cambridge, 2001).
24. R. Duncan-Jones, in *Approaching Late Antiquity: The Transformation from Early to Late Empire*, S. Swain, M. Edwards, Eds. (Oxford Univ. Press, Oxford, 2004), pp. 20–52.
25. C. Witschel, *J. Roman Archaeol.* **17**, 251 (2004).
26. D. J. Charman, A. Blundell, R. C. Chiverrell, D. Hendon, P. G. Langdon, *Quat. Sci. Rev.* **25**, 336 (2006).
27. L. B. Larsen *et al.*, *Geophys. Res. Lett.* **35**, L04708 (2008).
28. K. L. Kausrud *et al.*, *BMC Biol.* **8**, 112 (2010).
29. V. Trouet *et al.*, *Science* **324**, 78 (2009).
30. R. Brázdil, C. Pfister, H. Wanner, H. von Storch, J. Luterbacher, *Clim. Change* **70**, 363 (2005).
31. D. B. Lobell *et al.*, *Science* **319**, 607 (2008).
32. We thank E. Cook, K. Gibson, G. Haug, G. Huang, D. Johnson, M. Küttel, N. Stenseth, E. Zorita, and two anonymous referees for comments and discussion. Supported by the Swiss National Science Foundation (NCCR-Climate), the Deutsche Forschungsgemeinschaft projects PRIME (62201185) and Paleoclimatology of the Middle East (62201236), the Austrian Science Fund FWF (P15828, F3113-G02), l'Institut National de Recherches Archéologiques Préventives, the Andrew W. Mellon Foundation, and European Union projects MILLENNIUM (017008), ACQWA (212250), and CIRCE (036961).

Supporting Online Material

www.sciencemag.org/cgi/content/full/science.1197175/DC1
Materials and Methods
Figs. S1 to S12
Tables S1 and S2
References

31 August 2010; accepted 5 January 2011
Published online 13 January 2011;
10.1126/science.1197175

Passive Origins of Stomatal Control in Vascular Plants

Tim J. Brodribb* and Scott A. M. McAdam

Carbon and water flow between plants and the atmosphere is regulated by the opening and closing of minute stomatal pores in surfaces of leaves. By changing the aperture of stomata, plants regulate water loss and photosynthetic carbon gain in response to many environmental stimuli, but stomatal movements cannot yet be reliably predicted. We found that the complexity that characterizes stomatal control in seed plants is absent in early-diverging vascular plant lineages. Lycophyte and fern stomata are shown to lack key responses to abscisic acid and epidermal cell turgor, making their behavior highly predictable. These results indicate that a fundamental transition from passive to active metabolic control of plant water balance occurred after the divergence of ferns about 360 million years ago.

The evolution of stomata at least 400 million years ago (1) enabled plants to transform their epidermis into a dynamically permeable layer that could be either water-tight under dry conditions or highly permeable to

photosynthetic CO₂ during favorable conditions. The combination of adjustable stomata with an internal water transport system was a turning point in plant evolution that enabled vascular plants to invade most terrestrial environments

(2). Today, the leaves of vascular plants possess arrays of densely packed stomata, each one comprising a pair of adjacent guard cells (Fig. 1). High turgor pressure deforms the guard cells to form an open pore, which allows rapid diffusion of atmospheric CO₂ through the epidermis into the photosynthetic tissues inside the leaf. Declining turgor causes the guard cells to close together, greatly reducing leaf water loss while also restricting entry of CO₂ for photosynthesis. Despite the anatomical simplicity of the stomatal valve, there is little consensus on how angiosperm stomata sense and respond to their extrinsic and intrinsic environment. Because stomata are the gatekeepers of terrestrial photosynthetic gas exchange, understanding their dynamic control is imperative for predicting CO₂

School of Plant Science, University of Tasmania, Private Bag 55, Hobart, Tasmania 7001, Australia.

*To whom correspondence should be addressed. E-mail: timothyb@utas.edu.au



Supporting Online Material for

2500 Years of European Climate Variability and Human Susceptibility

Ulf Büntgen,* Willy Tegel, Kurt Nicolussi, Michael McCormick, David Frank, Valerie Trouet, Jed O. Kaplan, Franz Herzig, Karl-Uwe Heussner, Heinz Wanner, Jürg Luterbacher, Jan Esper

*To whom correspondence should be addressed. E-mail: buentgen@wsl.ch

Published 13 January 2011 on *Science Express*
DOI: 10.1126/science.1197175

This PDF file includes:

Materials and Methods

Figs. S1 to S12

Tables S1 and S2

References

Materials and methods

Oak data. Annually resolved oak ring width measurement series from three regions (Northeast France = NEF; Northeast Germany = NEG; Southeast Germany = SEG; Table S1) in Central Europe (CE) were compiled to continuously span the past ~2500 years and cover a large fraction of temperate forest area north of the Alpine arc and south of the Baltic Sea. The material contains oak (*Quercus robur* L. and *Q. petraea* (Matt.) Liebl.) wood from archaeological, sub-fossil, and historical surveys, as well as from recent findings. The CE oak species, *Q. robur* L. and *Q. petraea* (Matt.) Liebl., are not anatomically distinguishable (1). The historical portion of the oak dataset, which clearly represents the majority of the samples (Table S1), reaches continuously from the Iron Age to the early 20th century. We extended this dataset into the 21st century following a new approach to overcome the ‘update desideratum’ of modern site bias: adaptation of the recent to the historical data that was recently introduced by (2). In this case, recent oak beams and timber were randomly sampled at different sawmills and lumberyards scattered over the same area from which the historical

wood were derived. This random sampling strategy lowers site control and ecological understanding of the recent material, and typically results in artificial signal-degradation throughout the modern calibration period. It therefore helps to balance uncertainty-levels over multi-centennial to millennial-long tree-ring records composed of recent and historical wood material, and prevents from statistical over-fitting during the proxy/target calibration interval that ironically coincides with the industrial era (2).

Data adaptation. The three regional oak ring width subsets (NEF, NEG, SEG) and their CE mean compilation (ALL) were reduced in sample size, i.e., adapted, to test for possible effects of temporal replication changes on chronology behaviour (Fig. S1, S7; Table S1). The NEF data were reduced from originally 2880 to an adapted version of only 1025 series. The NEG data were reduced from 1785 to 833 series, the SEG data from 2619 to 779 series, and the CE mean dataset (ALL) from 7284 to 2637 series. This data adaptation procedure during which no new series were created, resulted in a more even distribution of individual series start and end dates throughout the past ~2500 years (Fig. S1), associated with a more homogeneous sample replication over time (Fig. S7C). Removal of samples from the original to the adapted datasets followed a random series selection process applied on highly-replicated pre-industrial periods from ~200 BC to AD 200, ~AD 400-900 and ~1000-1800, to roughly match sample size levels of the low-replication intervals from ~AD 200-400, as well as the 10th and 19th centuries (Fig. S1, Fig. S7C). The resulting adapted datasets and their subsequent oak chronologies (see below) allowed testing for biases introduced by temporal changes in sample size. The adaptation method further enabled us to consider possible uncertainties that might emerge from the integration of predominantly juvenile (fast growing) or mature/adult (slow growing) wood during specific periods of time.

Growth-trend analysis. Alignment of all individual raw ring width measurement series by their innermost ring, ideally representing the cambial age, facilitated the assessment of growth trends and levels (3). The resulting growth curves of the three regions, the so-called Regional

Curves (RCs) commonly describe trends of negative exponential shape (3), with very little differences between the original and adapted subsets (Fig. S2A). An assessment of the mean segment length (MSL) and average growth rate (AGR) of the raw measurement series indicated that shorter oak series, containing a greater fraction of juvenile wood, are characterized by overall higher growth rates, whereas longer series of more mature and adult wood contain generally lower growth rates (Fig. S2B). This commonly observed association between MSL and AGR in the raw ring width series emphasizes the need for tree-ring standardization (detrending) prior to any meaningful interpretation of externally forced variations (i.e., the putative climatic signal within the oak ring width data must be separated from the prevailing background noise). The observed similarities in AGR and consistency in the MSL/AGR association among the various regional subsets denoted their compatibility also with respect to growth rates and trends.

High-frequency preservation. To maintain inter-annual (high-frequency) variability from the three regional oak ring width subsets (NEF, NEG and SEG), the original and adapted subsets of raw measurement series were standardized, i.e., detrended using individual cubic smoothing splines with 50% frequency-response cut-off at 20 years (4). This detrending approach has been demonstrated to robustly preserve growth extremes while eliminating background noise on inter-decadal and longer time-scales (5). Annual ring width indices were herein calculated as ratios, but also as residuals after the application of a data adaptive power-transformation applied on the raw measurement series (6). A bi-weight robust mean was used to generate regional-scale subset chronologies of high-frequency variability. The various oak chronologies (ratios/original; residuals/original; ratios/adapted; residuals/adapted) per region were truncated at a minimum replication of five series and normalized over their individual length. To minimize biases due to replication and inter-series correlation changes, the normalized time-series were additionally corrected for artificial variance changes by calculating ratios from 31-year moving standard deviations (7), i.e., the normalized annual

chronology indices were divided by the corresponding values of their 31-year moving standard deviations (Fig. S3). The variance stabilized, regional-scale (high-frequency) chronologies are most suitable to detect inter-annual growth extremes likely caused by hydroclimatic anomalies. Nevertheless, they do not contain any information about longer-term changes in the prevailing climate system or their surrounding environment (5).

Extreme-year validation. We calculated moving 31-year correlation coefficients to assess the shared inter-annual (high-frequency) variability amongst the three regional subset chronologies (Fig. S4A). Correlation coefficients amongst the three time-series average at 0.44 over the common 210 BC to AD 1992 period. Higher agreement of $r = 0.52$ was found over the better-replicated last millennium. Reduced coherency amongst the three regional chronologies occurred from ~1800 onwards, the period during which the randomly updated recent data prevail. This recent coherency decline indicates that the proxy/target calibration results (see below) are likely conservative (2). The variance stabilized high-frequency chronologies (Fig. S4B) were further used to reconstruct the frequency and severity of annual growth extremes, which either occurred at the regional-scale, i.e., in two of the three regional chronologies, or at the sub-continental CE-scale, i.e., common to all three regional oak chronologies (Fig. S4C). Regional extremes in radial oak growth were defined as occurring when all four chronologies per region (ratios/original; residuals/original; ratios/adapted; residuals/adapted) exceeded their corresponding 1.5 standard deviation threshold (5). Sub-continental CE network extremes occurred when all three regional records shared an extreme year.

Scaled precipitation anomaly (1961-1990 mean subtracted) composites (8) for CE summers (June-August) were computed for the oak extremes back to AD 1500 (Fig. S5). In contrast to the classical compositing technique that uses the arithmetic mean and a t-test for the means, we applied a scaled mean and modified t-value (8). This method provides more robust results if the distribution is not 'Gaussian', in case of small samples or if there are

outliers. Scaled anomaly composites were calculated for the 12 most positive and the 16 most negative oak extremes back to AD 1500 using gridded precipitation reconstructions (9).

We extracted historical documentary evidence assembled and uploaded to the geo-database ‘Digital Atlas of Roman and Medieval Civilizations’ (DARMC; <http://darmc.harvard.edu>), to verify the climatic signal in the oak extremes further back in time, i.e., during the first half of the last millennium during which no gridded precipitation reconstructions exist (9). The early historical records in Latin, Middle Dutch, Middle French, and Middle German supplied a total of 87 different medieval records, usually eyewitnesses from or near the regions represented by the oak network. The 87 different records offered 104 reports (since some records report on multiple years) on regional hydroclimatic conditions in 32 extreme years, resolved to the year or better, with 1-7 witnesses per year. A total of 88 out of 104 reports corroborate 30 out of 32 of the precipitation extremes preserved in our oak record between 1013 and 1504. Of the 16 contradictory reports, 13 occur for 9 years (AD 1221, 1270, 1309, 1350, 1353, 1368, 1434, 1464, 1487) whose precipitation extremes are in fact corroborated by 20 (of the 88) confirming historical witnesses. The contradictory reports for those 9 years may reflect local precipitation variation or simply ambiguity in those medieval written records. The only three reports that contradict the dendro-data in the absence of other, corroborating testimony, refer to two poorly documented years (AD 1044, 2 reports, and 1121, 1 report). Thus the medieval human witnesses independently confirm the skill of our method for reconstructing precipitation from the proxy data in a time and region where the anthropogenic impact on climate systems and mechanisms was minimal.

Three independently developed oak chronologies from Great Britain and Northern Germany (10), from Central Germany (11) and from Slovenia (12) were re-processed here, i.e., 20-year high-pass filtered, and then used for comparison with our new high-frequency oak data, both at the regional-scale and the CE network level (Fig. S6).

Tree-ring detrending. The three regional datasets including their original and adapted versions were horizontally split into recent and historical oak samples (2, 11), and processed using various detrending methods. This approach helped us not only to best maintain high- to low-frequency hydroclimatic variability, but also to detect and account for biologically induced age trends (4, 6), population biases (3), and recent chronology characteristics (2, 11). Aligning the raw ring width measurement series by cambial age revealed common age trends in the NEF, NEG and SEG oak data. This alignment further demonstrated coherent relationships between MSL and AGR amongst the three regions (Fig. S2). Possible chronology biases related to changes in sample size and tree population have been discussed in the light of data adaptation (Fig. S1). Uncertainty associated with the most recent end of tree-ring chronologies that might emerge from exceptional changes in concentrations of atmospheric greenhouse-gases, levels of biospheric fertilization, the amount of forest management and degree of habitat opening (2), as well as end-effect problems in chronology behaviour (6), are most likely relevant for lower elevation temperate oak forest across CE (11), and thus justify horizontal data splitting into recent and historical subsets prior to their detrending (Table S1) (see also description below).

An array of eight different detrending methods using individual cubic smoothing splines with 50% frequency-response cut-off at 150 years (4) and alternatively using the Regional Curve Standardization (RCS) method (3), either based on ratios or residuals and utilizing the original or adapted datasets (ratios/original; residuals/original; ratios/adapted; residuals/adapted) was employed to test for possible effects on the resulting ring width chronologies. Note that correlation coefficients amongst the three regional (historical RCS/recent spline) chronologies either using the original or the adapted data (i.e., original versus adapted) average at 0.94 over the past two millennia. Correlation coefficients amongst the three regional (historical RCS/recent spline) chronologies either using ratios or residuals after power-transformation (i.e., ratios versus residuals) average at 0.93 over the past two

millennia. The different chronology versions (original versus adapted) after 150-year spline detrending show rather similar inter-annual to multi-decadal variations (Fig. S7). The corresponding Expressed Population Signal (EPS) values constantly range above the commonly applied threshold of 0.85 back to ~300 BC. No differences in mean EPS over the full period have been found between the original (0.97; 7284 series) and adapted (0.95; 2637 series) datasets (Fig. S7A). The EPS statistic, however, mainly verifies the high-frequency coherence of the oak measurements and potential changes in the wood source material that are common to the original and adapted datasets may still imply some non climatic noise. The 95% bootstrap confidence intervals of the original and adapted oak chronologies after 150-year spline detrending further reveal similar results (Fig. S7B), suggesting that the chronology behaviour is robust over time, and biases due to temporal changes in sample size are negligible. The chronologies (original/adapted) correlate at 0.93 with each other back to 400 BC, even though their replication substantially differs (Fig. S7C).

Some offset between the different tree-ring detrending and chronology development techniques was, however, found during the 20th century (Fig. S8). Those chronologies that were based on 150-year spline detrending contain less positive trends and best resembled the nearly trend-free gridded precipitation indices. Those chronologies that were developed with the RCS method and thus allow lower frequency variation to be preserved though indicate long-term growth increases over 1901-2006, possibly induced by effects of modern changes in forest management and cultivation, as well as further biases predominantly associated with the industrial period and recent end of tree-ring records including increased atmospheric greenhouse-gas, biospheric fertilization, sample replication, age-structure and chronology development. See (2) for a description of such effects and techniques to overcome them. We therefore considered the recent subsets of the three regions (NEG, NEF, SEG) after they were detrended with individual 150-year cubic smoothing splines combined with the RCS detrended historical series as the best method presently available to preserve hydroclimatic

information in an oak ring width chronologies. Similar techniques were applied in a comparable, but independent study from Central Germany (11).

Nevertheless, we are aware of the compromise this step implies: while minimizing biases that are most critical during the recent section of the millennial-long oak chronologies, the approach of horizontal splitting and using different detrending techniques at the same time limits the comparison of historical and recent information, and possible conclusions about the comparatively small hydroclimatic variations inferred for the recent period. Nevertheless, we believe this to be less critical, since our study mainly focuses on pre-industrial climate change. The historical subsets of the three regions were therefore detrended with the RCS method to maintain possible low-frequency information on time-scales exceeding those of the individual series lengths (13). This approach of horizontally different detrending, i.e., composite RCS for the historical samples and individual spline for the recent samples, was applied, as the recent chronology portion possibly contains biases (as discussed earlier), some of which are unique to the past ~150 years and the lower elevation temperate CE forests (2). Changes in forest management and habitat cultivation yielding increased forest productivity, via enhanced tree growth – which we believe to be most critical factors, however, possibly were less severe during earlier periods, but certainly were negligible for natural stands near the upper elevational treeline in the European Alps, for example, where human interventions played and play a less important role (see below). The recent spline and historical RCS chronologies were annually weighted by their sample replication and averaged. Note that even though the horizontal split approach may reduce some longer-term biases in the chronology (11, 14), it can possibly also diminish lower frequency information within the shorter recent subsets (13). This methodological constraint may complicate any straightforward comparison between modern industrial and earlier pre-industrial hydroclimatic variability.

Precipitation reconstruction. Due to non-significant differences between chronologies based on either the original or the adapted datasets, as well due to using ratios or residuals

after power-transformation for index calculation, it appeared unjustified to select a ‘single best solution’ and we therefore developed three regional-scale mean records considering information from the four minimally different chronologies. The three mean regional chronologies, including information from historical RCS chronologies and recent spline chronologies using ratios as well as residuals after power-transformation for indexing, were annually weighted by their individual sample replications and averaged to form a CE mean oak chronology. This procedure allowed us to firstly assess growth rates, trends and responses at the regional-scale, to secondly compare those parameters amongst the three regions as well against independent existing chronologies, and to finally compile regional evidence in a sub-continental network. It should further be noted that the region from where the NEF data are derived was under Roman occupation, that NEG region was never under Roman occupation and that SEG was at a border region.

We applied growth-climate response analyses of the new CE mean oak chronology using monthly resolved precipitation totals (mm/day) averaged over the 6-12° E and 48-52° N CE region (*16*) (Fig. S9). Previous year precipitation showed no impact on oak growth, whereas monthly totals of April, May and June revealed positive correlations (Fig. S9C). April-June (AMJ) precipitation totals revealed the highest positive correlation, significant at the 99.9% confidence limit (1901-1980), and were subsequently used for reconstruction purposes. To avoid regression-based variance reduction in the proxy reconstruction model (*15*), the CE mean oak chronology was scaled (1901-1980) against April-June (AMJ) precipitation totals (mm) averaged over the 6-12° E and 48-52° N CE region (*16*). This ‘composite plus scaling’ procedure, i.e., the adjustment of proxy mean and variance, is the simplest amongst various calibration techniques but is perhaps also least prone to variance underestimation (for a more detailed discussion see *15*, *17*). The relationship between radial oak growth and AMJ precipitation was tested for temporal and spatial stability (Fig. S9). Field correlation analyses between the oak chronology and gridded precipitation indices (*16*) were performed for the

European sector (Fig. S9D). The spatial signature of the oak proxy was compared with the idealized spatial correlation field obtained from the mean of three instrumental precipitation target records that best represent the location of the tree oak sample regions (i.e., stations from Nancy, Regensburg and Potsdam). Uncertainty bars of the final reconstruction reflect the ± 1 root mean square error (RMSE) computed from the calibration period.

Temperature reconstruction. A total of 1546 ring width series from high-elevation conifers sampled in the Austrian Alps, mainly Tyrol and adjacent areas was aggregated. This compilation describes an updated subset of a near Holocene-long tree-ring network of sub-fossil wood, historical timber and recent trees (18). The dataset contains the two dominant Alpine treeline species Stone pine (*Pinus cembra*) and European larch (*Larix decidua*), with their radial growth being dominated by summer temperature variability (14). A total of 1089 series represents pine trees and 457 series represent larch trees, either containing the pith or allowing pith-offsets to be estimated. The combined dataset is characterized by sufficient sample size, i.e., a mean of 109 series per year over the past 2500 years (Fig. S10). Constant replication of >100 series is given from AD 1249 onwards, whereas a sample size of >30 series reaches back to AD 134.

Data were horizontally separated, RCS detrended, weighted averaged and scaled against homogenized JJA temperature means of the great Alpine region (19,20) and the 1864-2006 period (Fig. S11). A similar approach and interval has been previously demonstrated to allow variations in Alpine summer temperature to be robustly reconstructed for the past 1250 years (21). Field correlation analysis (22) between the new Alpine conifer chronology and gridded JJA temperature indices (16) was performed over the European sector (Fig. S12). Uncertainty bars refer to the ± 1 RMSE derived from the calibration period.

Figures and tables

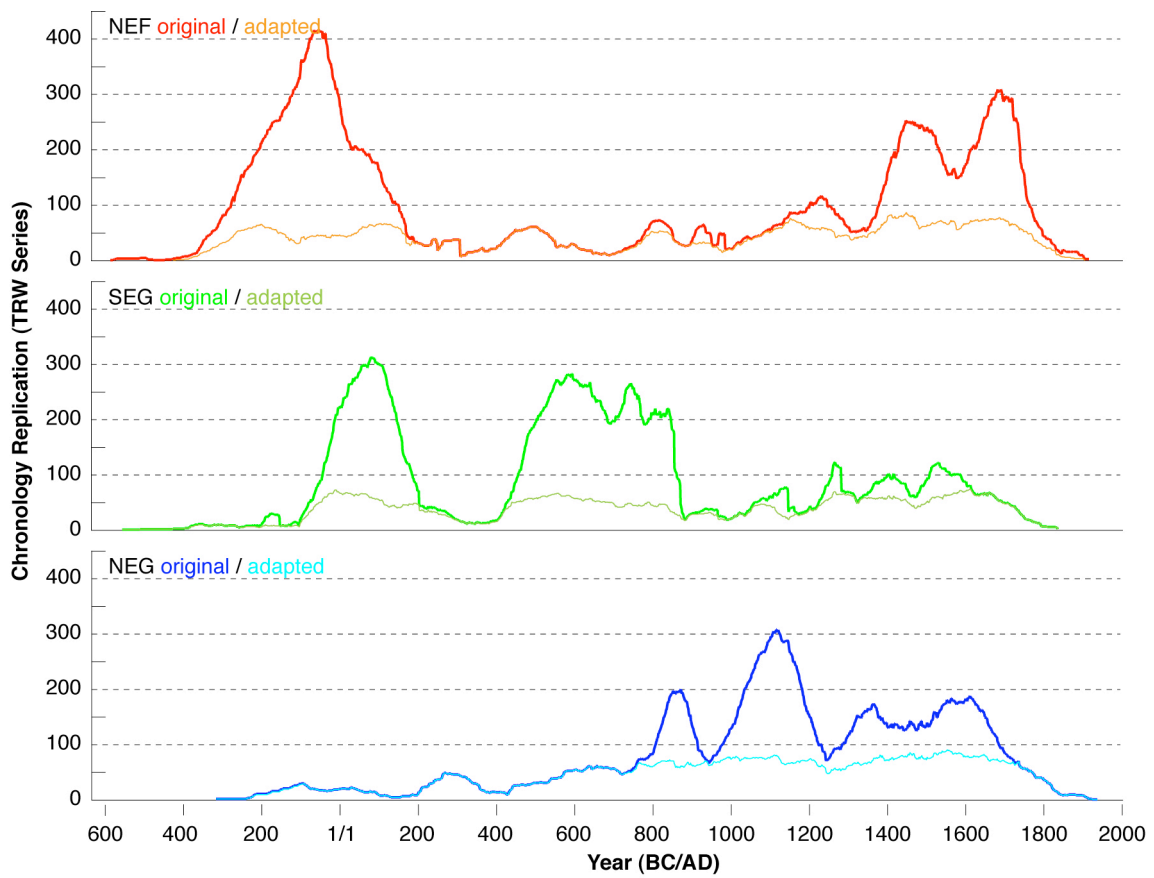


Fig. S1. Series replication of the three historical oak datasets (NEF, SEG, NEG), using either their original or adaptation subsets (see table S1 and figure S7 for details).

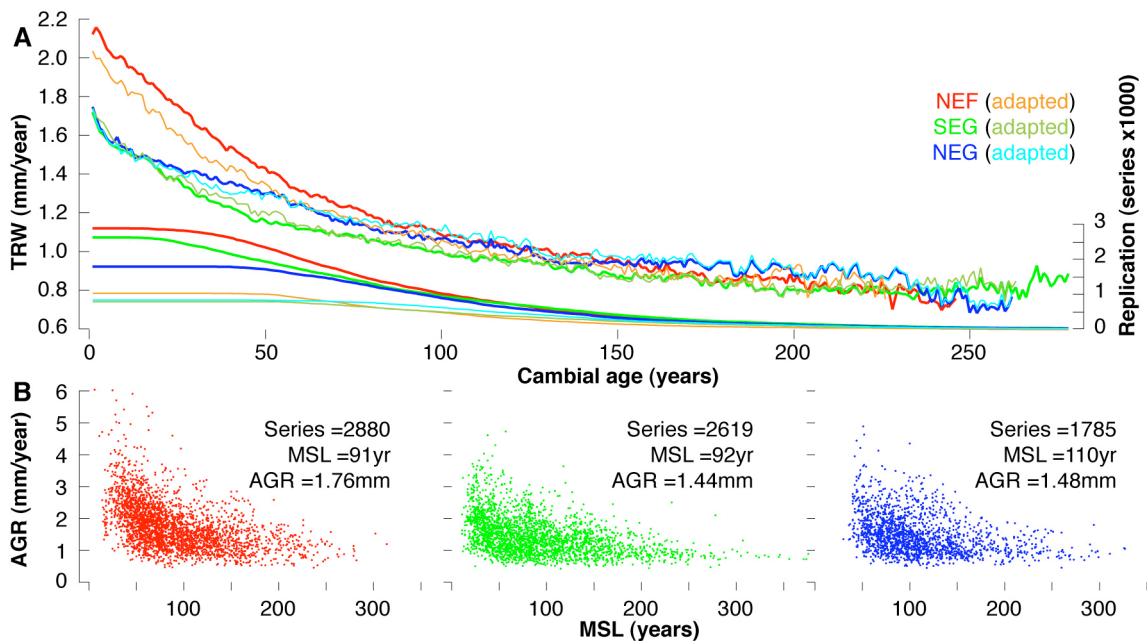


Fig. S2. (A) Regional Curves of the age-aligned TRW measurement series and their replication using the original and adapted regional sub-sets (see table S1 for details). **(B)** Relationship between average growth rate (AGR) and mean segment length (MSL) of the 7284 oak samples geographically divided into the three regional sub-sets (Northeast France = NEF, Southeast Germany = SEG, Northeast Germany = NEG).

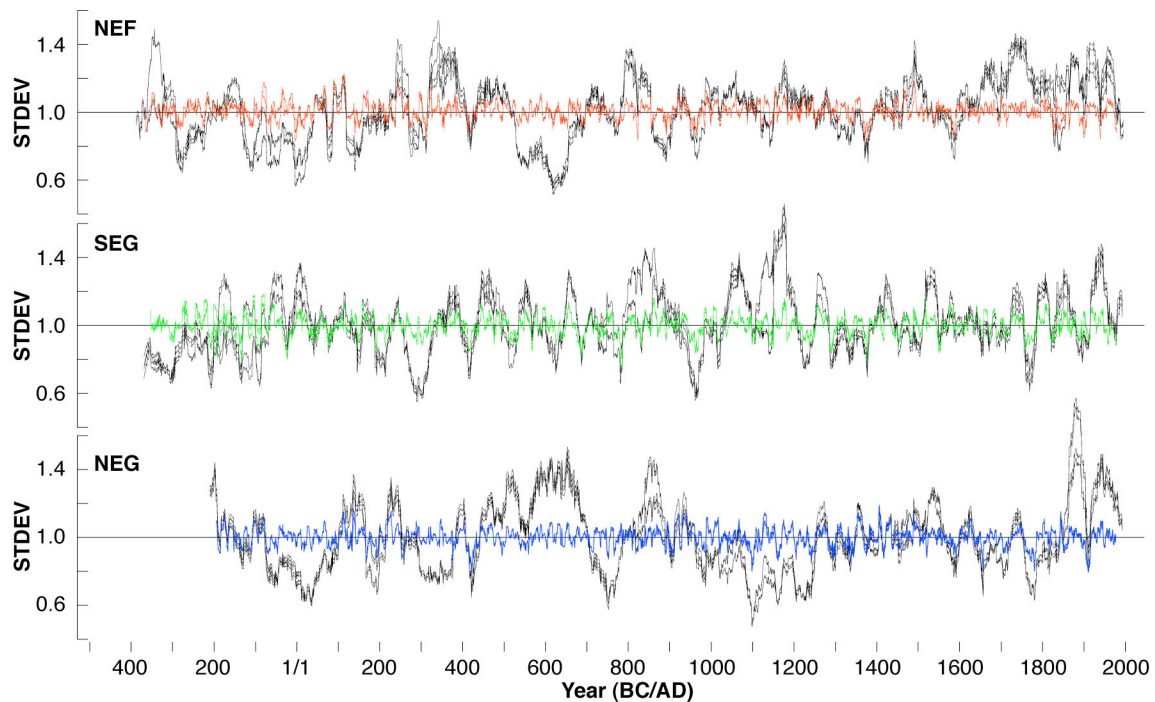


Fig. S3. Moving 31-year standard deviations of the three regional high-frequency chronologies (after 20-year spline detrending with and without power-transformation and using the original and adapted subsets) before (black) and after (color) variance stabilization.

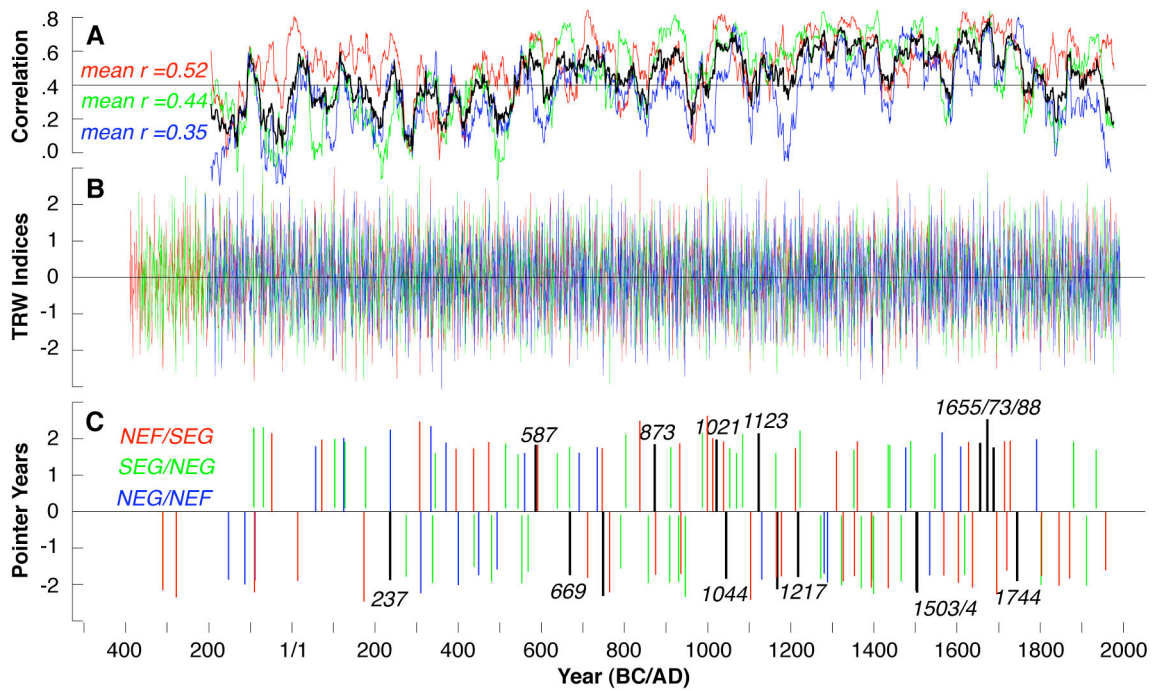


Fig. S4. (A) Moving 31-year correlations and Rbar (black) between (B) the regional sub-set chronologies (after 20-year spline detrending and variance stabilization), and (C) positive and negative extremes amongst the entire network (black) and the regional sub-sets.

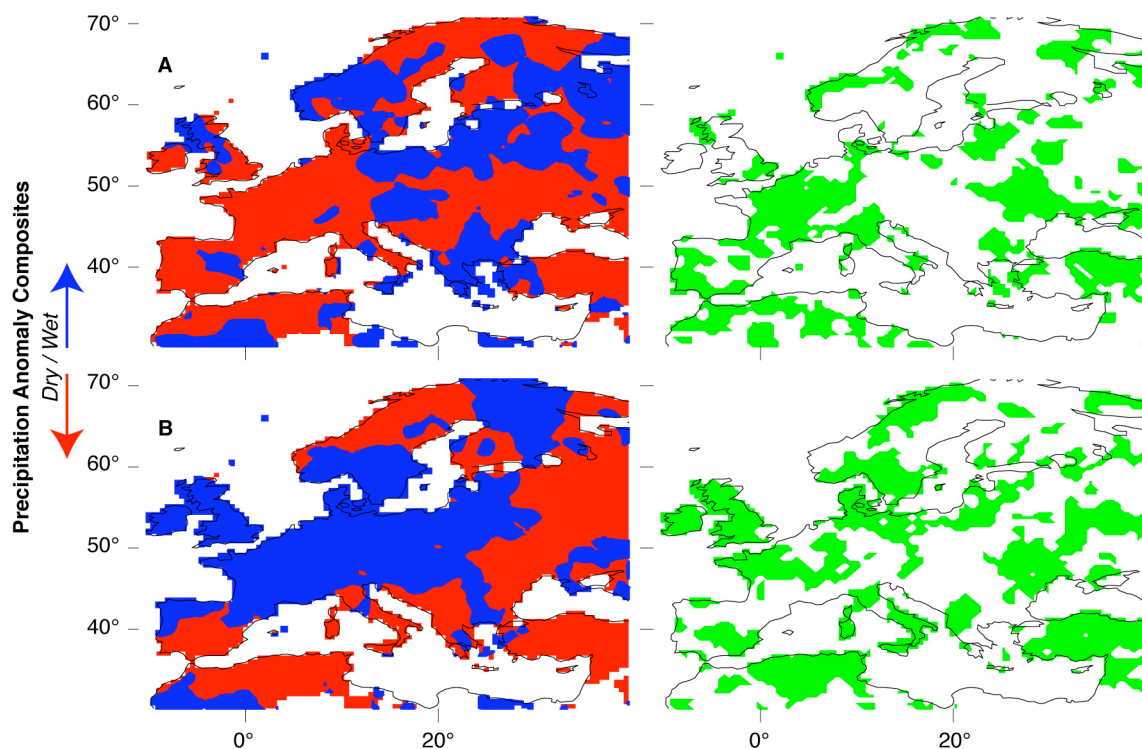


Fig. S5. Scaled anomaly composites (δ) of summer precipitation (θ) computed for (A) the 16 negative and (B) the 12 positive oak extremes between AD 1500 and 2000.

Blue and red colours refer to wet and dry conditions. The green shadings (**Right**) indicate the 95% confidence levels.

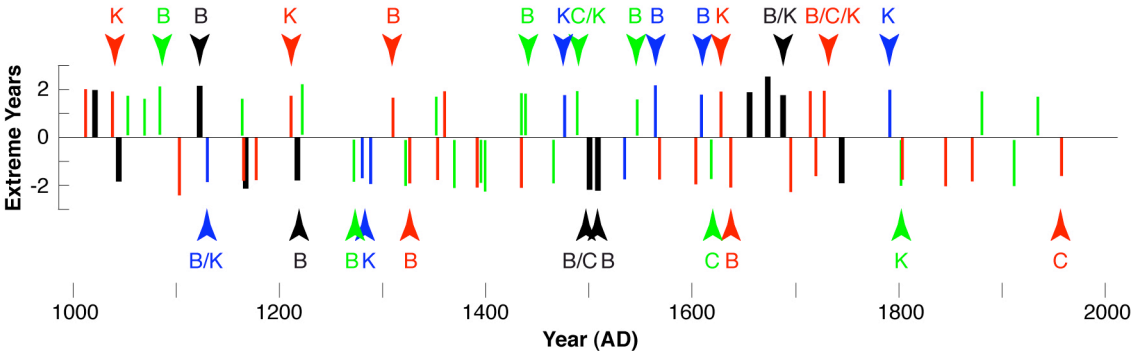


Fig. S6. Positive and negative oak extremes that either occurred over the entire network (black), or were restricted to the three regional subsets NEF/SEG (red), NEG/NEF (green) and SEG/NEG (blue) back to 1000. Corresponding colour-arrows refer to independent oak data from Central Germany (11; 1063-1990; B), Slovenia (12; 1497-2003; C) and Great Britain (10; 0-1996; K) that show similar growth extremes.

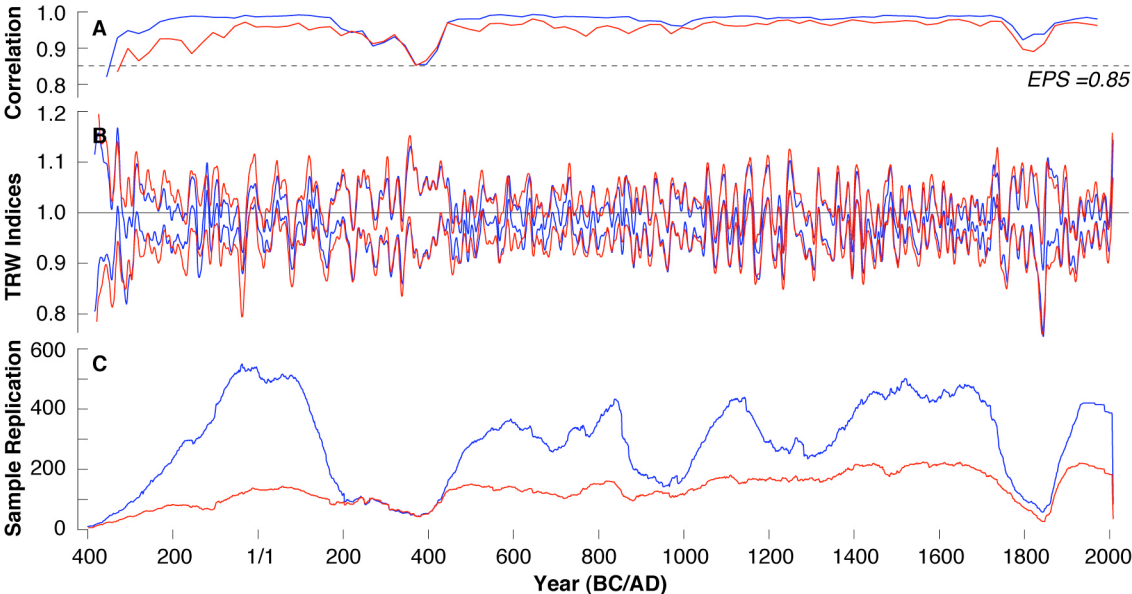


Fig. S7. (A) The Expressed Population Signal (EPS) of the original (blue; 7284 series) and adapted (red; 2637 series) oak chronologies, computed over 50-year periods and shifted by 25 years back in time. (B) The 95% bootstrap confidence intervals of the original (blue) and adapted (red) oak chronology after 150-year spline detrending. The time-series are 20-year low-pass filtered. (C) Series replication of the original (blue) and adapted (red) chronologies.

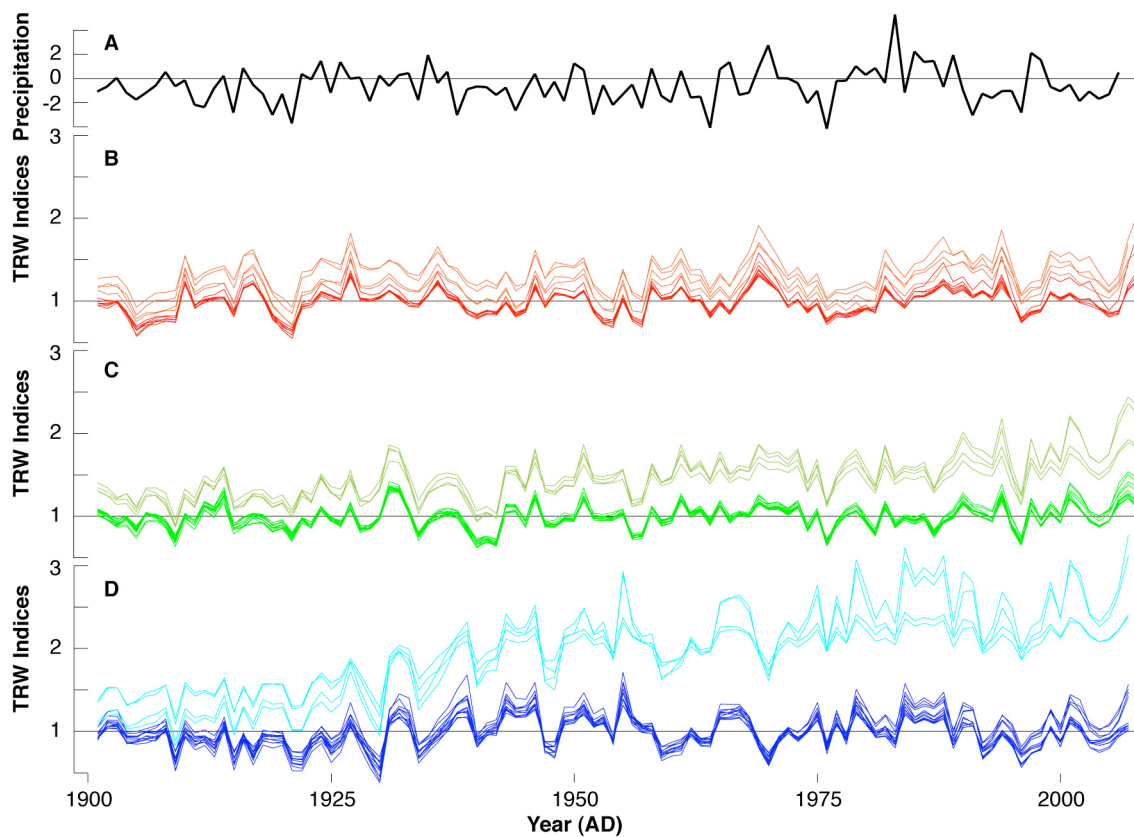


Fig. S8. (A) Precipitation anomalies (mm/day with respect to 1961-1990; CRUTS3) averaged over the 6-12° E and 48-52° N CE region, compared with different chronology versions of the three regional subsets: (B) NEF, (C) SEG and (D) NEG. The light colors refer to four RCS chronologies (ratios/original; residuals/original; ratios/adapted; residuals/adapted) that allow trend biases to occur, whereas the bright colors refer to the corresponding four chronology versions after 150-year spline chronologies that prevent possible biases during the recent time-series ends.

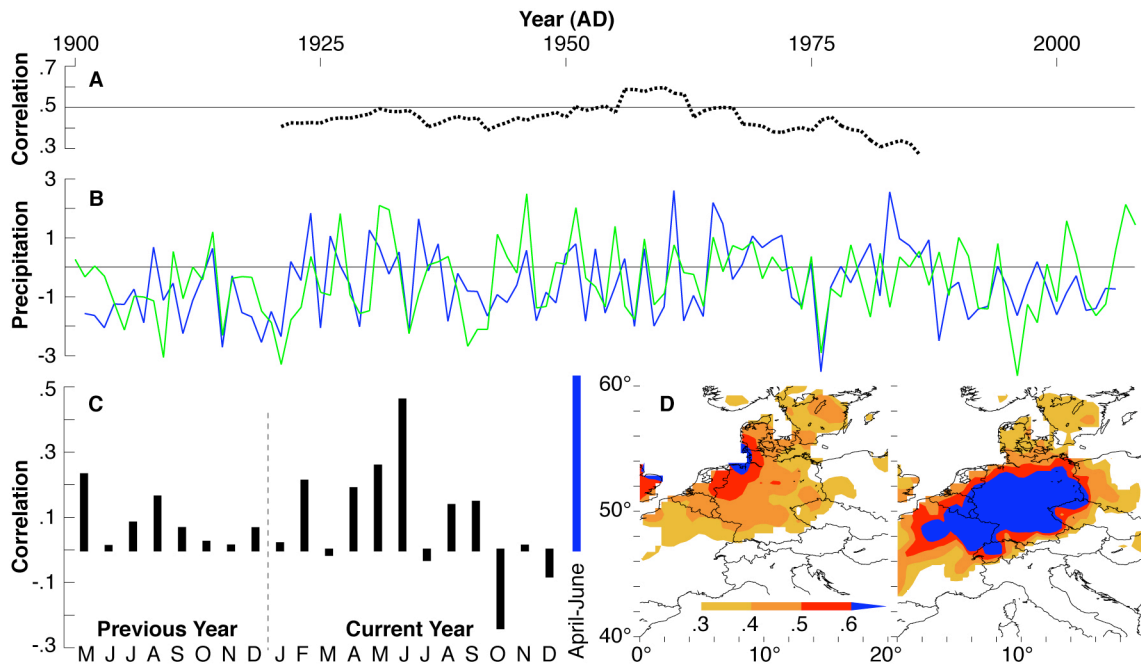


Fig. S9. (A) Moving 31-year correlations between AMJ precipitation (averaged over 6-12° E and 48-52° N) and the mean CE oak chronology. (B) Measured (blue) and reconstructed (green) AMJ precipitation anomalies (mm/day with respect to 1961-1990; CRUTS3) after scaling over the 1901-1980 period. (C) Correlations between monthly precipitation totals and the oak chronology (1901-1980), and (D) spatial Spearman correlations of the oak chronology against gridded (0.5°x0.5°) AMJ precipitation anomalies. The right map shows spatial correlations of the mean of three instrumental stations (Nancy, Regensburg, Potsdam) best representing the oak sub-regions against gridded (0.5°x0.5°) AMJ precipitation anomalies.

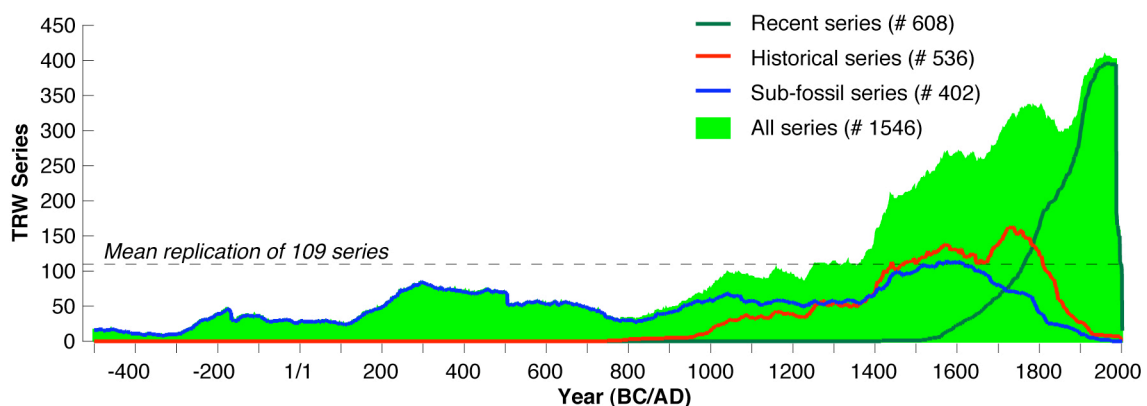


Fig. S10. Temporal distribution of the 1546 Alpine conifer ring width series from the Austrian Alps, classified into recent, historical and sub-fossil material, which have been used to reconstruct JJA temperature variability.

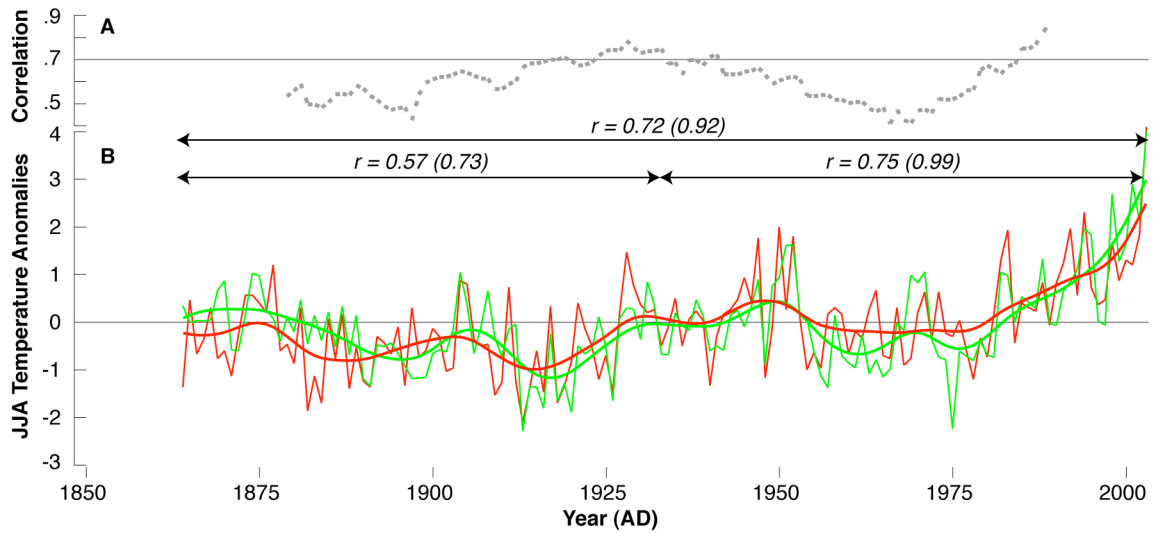


Fig. S11. (A) Moving 31-year correlations between the measured JJA temperatures of the Greater Alpine Region (20,21) and the Alpine conifer chronology. **(B)** Measured (red) and reconstructed (green) JJA temperature ($^{\circ}\text{C}$) anomalies (wrt. 1961-1990) after scaling over the reliable 1864-2003 period of proxy/target overlap. The smoothed lines are 20-year low-pass filtered, corresponding to correlations in brackets.

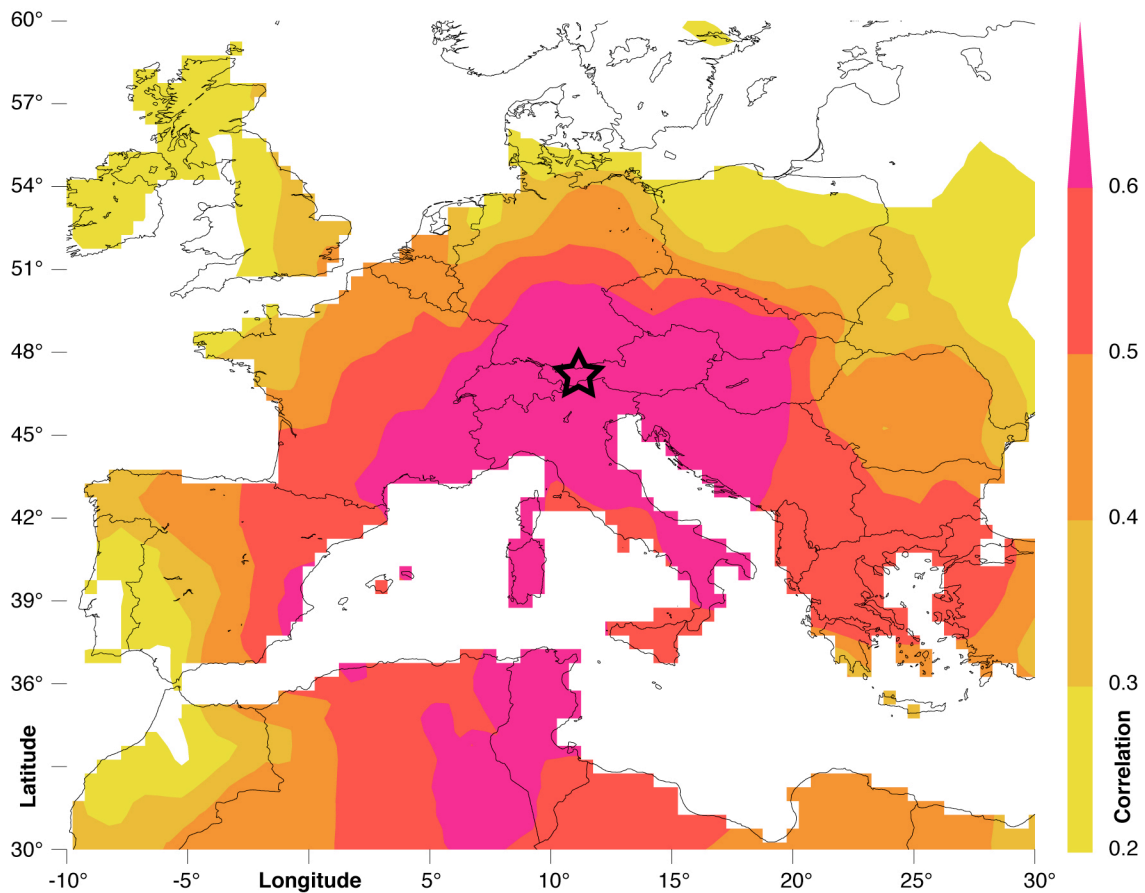


Fig. S12. Spatial signature of the new CE JJA temperature reconstruction (black star) expressed as field correlations against gridded 0.5°x0.5° JJA temperatures (16) computed over the 1901-2003 period.

Table S1. Summary information of the oak ring width data used in this study. The inventory of the entire dataset (7284 series; ALL) is further divided into regional (NEF, NEG, SEG) and horizontal (recent and historic) subsets, considering the original (black) and adapted (grey) data versions. MSL = Mean segment length; AGR = Average growth rate; AC1 = First order autocorrelation; Start/End >5 = Chronology start and end dates with a sample replication >5 series; NEF = Northeast France; NEG = Northeast Germany; SEG = Southeast Germany.

Dataset	Series	Length	MSL	AGR	AC1	Start >5	End >5
ALL	7284	2597	98	1.559	0.605	405BC	2008AD
NEF	2880	2597	91	1.757	0.622	405BC	2008AD
SEG	2619	2565	92	1.437	0.549	384BC	2008AD
NEG	1785	2326	110	1.482	0.644	225BC	2007AD
NEF-adapted	1025	2437	103	1.523	0.661	379BC	2007AD
SEG-adapted	779	2565	128	1.319	0.649	203BC	2008AD
NEG-adapted	833	2326	136	1.409	0.671	225BC	2007AD
NEF-historic	2813	2503	90	1.758	0.62	405BC	1902AD
NEF-recent	67	273	153	1.714	0.69	1795AD	2008AD
SEG-historic	2394	2392	90	1.41	0.545	253BC	1829AD
SEG-recent	225	202	114	1.745	0.59	1846AD	2008AD
NEG-historic	1657	2254	109	1.42	0.638	225BC	1906AD
NEG-recent	128	296	120	2.273	0.718	1861AD	2007AD
NEF-historic-adapted	965	2333	103	1.517	0.663	379BC	1868AD
SEF-historic-adapted	692	2392	127	1.281	0.654	245BC	1829AD
NEG-historic-adapted	755	2254	136	1.335	0.665	225BC	1906AD
SEG-recent-adapted	87	202	131	1.616	0.605	1850AD	2008AD
NEG-recent-adapted	77	296	133	2.124	0.717	1859AD	2007AD

Table S2. Inventory of the annual oak growth extremes detected at the overall CE and the regional-scales over the entire time-series spans. B covers the AD 1063-1990 (11); C covers the AD 1497-2003 (12); K covers the AD 0-1996 (10); * have been used for the anomaly composites.

Central Europe positive / negative		NEF / SEG positive / negative		NEF / NEG positive / negative		SEG / NEG positive / negative	
587	237	-49	-311	56	-114	-70	-93
873	669	71	-279	123	-90	102	273
1021	749	307	-91	235 K	308K	126K	337
1123B	1044	395	13	333	399K	176K	437K
1655*	1167	436	173K	369	448K	344	478
1673*BK	1217B	473K	711K	393	492	512K	551K
1688*	1503*CB	590	764	558	1129BK	542K	566
	1504*C	746	874 K	690	1278	637	790
	1744*	837	935	733	1287K	666	855
		932	1102	1474K	1532*	802	907
		999	1165	1562*B		909	928
		1013	1177	1607*B		985	945
		1037K	1326B	1789*K		1052	1270B
		1210K	1353			1068	1320
		1309B	1393			1082B	1368
		1359	1434			1163	1394
		1627*K	1567*			1221	1397
		1713*	1603*			1350	1464
		1727*BCK	1636*B			1433	1616*C
			1695*			1436B	1800*K
			1719*			1487B	1909*
			1802*			1545*CK	
			1845*			1879*	
			1870*			1932*	
			1957*C				

References

1. K. Haneca, K. Čufar, H. Beeckman, Oaks, tree-rings and wooden cultural heritage: a review of the main characteristics and applications of oak dendrochronology in Europe. *J. Archaeol. Sci.* **36**, 1-11 (2009).
2. W. Tegel, J. Vanmoerkerke, U Büntgen, Updating historical tree-ring records for climate reconstruction. *Quat. Sci. Rev.* **29**, 1957-1959 (2010).
3. J. Esper, E. R. Cook, P. J. Krusic, K. Peters, F. H. Schweingruber, Tests of the RCS method for preserving low-frequency variability in long tree-ring chronologies. *Tree-Ring Res.* **59**, 81-98 (2003).
4. E. R. Cook, K. Peters, The smoothing spline: A new approach to standardizing forest interior tree-ring width series for dendroclimatic studies. *Tree-Ring Bull.* **41**, 45-53 (1981).

5. G. Battipaglia, *et al.*, Five centuries of Central European temperature extremes reconstructed from tree-ring density and documentary evidence. *Glob. Planet. Change* **72**, 182-191 (2010).
6. E. R. Cook, K. Peters, Calculating unbiased tree-ring indices for the study of climatic and environmental change. *Holocene* **7**, 361-370 (1997).
7. D. Frank, J. Esper, E. R. Cook, Adjustment for proxy number and coherence in a large-scale temperature reconstruction. *Geophys. Res. Lett.* **34**, doi: 10.1029/2007GL030571 (2007).
8. T. J. Brown, B. L. Hall, The use of t values in climatological composite analyses. *J. Clim.* **12**, 2941-2945 (1999).
9. A. Pauling, J. Luterbacher, C. Casty, H. Wanner, 500 years of gridded high-resolution precipitation reconstructions over Europe and the connection to large-scale circulation. *Clim. Dyn.* **26**, 387-405 (2006).
10. P. M. Kelly, H. H. Leuschner, K. R. Briffa, I. C. Harris, The climatic interpretation of pan-European signature years in oak ring-width series. *Holocene* **12**, 689-694 (2002).
11. U. Büntgen, *et al.*, Tree-ring indicators of German summer drought over the last millennium. *Quat. Sci. Rev.* **29**, 1005-1016 (2010).
12. K. Čufar, M. De Luis, D. Eckstein, L. Kajfez-Bogataj, Reconstructing dry and wet summers in SE Slovenia from oak tree-ring series. *Int. J. Biometeorol.* **52**, 607-615 (2008).
13. E. R. Cook, K. R. Briffa, D. M. Meko, D. A. Graybill, G. Funkhouser, The 'segment length curse' in long tree-ring chronology development for palaeoclimatic studies. *Holocene* **5**, 229-237 (1995).
14. U. Büntgen, J. Esper, D. C. Frank, K. Nicolussi, M. Schmidhalter, A 1052-year tree-ring proxy for Alpine summer temperatures. *Clim. Dyn.* **25**, 141-153 (2005).

15. J. Esper, D. C. Frank, R. J. S. Wilson, K. R. Briffa, Effect of scaling and regression on reconstructed temperature amplitude for the past millennium. *Geophys. Res. Lett.* **32**, doi: 10.1029/2004GL021236 (2005).
16. T. D. Mitchell, P. D. Jones, An improved method of constructing a database of monthly climate observations and associated high-resolution grids. *Int. J. Climatol.* **25**, 693-712 (2005).
17. D. C. Frank, *et al.*, Ensemble reconstruction constraints of the global carbon cycle sensitivity to climate. *Nature* **463**, 527-530 (2010).
18. K. Nicolussi, *et al.*, A 9111 year long conifer tree-ring chronology for the European Alps: a base for environmental and climatic investigations. *Holocene* **19**, 909-920 (2009).
19. I. Auer, *et al.*, HISTALP – Historical instrumental climatological surface time series of the greater Alpine region 1760-2003. *Int. J. Climatol.* **27**, 17-46 (2007).
20. R. Böhm, *et al.*, The early instrumental warm-bias: a solution for long central European temperature series 1760–2007. *Clim. Change* **101**, 41-67 (2010).
21. U. Büntgen, D. C. Frank, D. Nievergelt, J. Esper, Summer temperature variations in the European Alps, AD 755-2004. *J. Clim.* **19**, 5606-5623 (2006).
22. U. Büntgen, *et al.*, Assessing the spatial signature of European climate reconstructions. *Clim. Res.* **41**, 125-130 (2010).